

Physical and electrical characterization of silicon suboxide seed layer

Seref Kalem

Bahcesehir University, Electrical and Electronics Engineering, Ciragan Caddesi, Besiktas 34353
Istanbul, Turkey

ABSTRACT

The silicon suboxide SiO_x ($x < 2.0$) offers promising application possibilities ranging from electrodes in lithium-ion batteries used widely in electrical vehicles and portable devices to sensing applications. Therefore, a low cost, environmental friendly and high performance oxide materials are required for an appropriate operation of any electronic gadget. In this work, we report on the physical and electrical properties of a suboxide formed as a seed layer during the formation of a dielectric layer, namely the ammonium silicon hexafluoride. The measurement results reveal interesting properties, which are required to be understood clearly before any application. The results have been analyzed using state-of-the-art techniques and compared with the developments of SiO_x obtained by related techniques. In this presentation, a comprehensive review of the physical and electrical properties is given in order to clarify the origin of the observed features. At the end of the paper, a lookout is provided for the possible applications of this special SiO_x dielectric seed layer.

Keywords: Silicon sub-oxide, seed layer, energy dispersive x-ray, localized vibrational modes, photoluminescence, spectroscopic ellipsometry, resistive switching.

1. INTRODUCTION

The technical aspect of our research work is based on the investigation of physical and electrical properties of silicon suboxide seed layer grown during the ammonium silicon hexafluoride dielectric formation process [1]. The silicon suboxide in this process played the role of a seed layer for the growth of the dielectric. The removal of deionized water soluble dielectrics leaves the silicon suboxide on the surface of the silicon wafer. The oxide so grown has been subjected to a number of state-of-the-art characterization techniques.

Localized vibrational modes analysis revealed the presence of Si-TO and Si-O-Si stretching bands as well as TO-LO mode couplings. The presence of Si-H modes have also been identified in the silicon suboxide matrix prepared under certain conditions. CW and time-resolved photoluminescence (PL) measurements have exhibited a broad band emission ranging from the UV to mid-infrared region with decay times ranging from picosecond to nanosecond time scales. CW PL reveals an emission at around 700nm, which is well correlated with the seed layer thickness.

The spectroscopic ellipsometry provided us with the identification of the energy band structure through the presence of the critical point energy transitions. I-V characteristics of MOS devices are indicative of a resistive switching and electro-formation mechanism in the layers. The results have been analyzed using advanced correlation techniques.

The presentation will give a comprehensive summary of the development in this area in an attempt to evaluate the feasibility potential of silicon suboxide layer so grown for advanced applications.

2. EXPERIMENTAL

2.1 Growth conditions

Silicon suboxide layer was formed during the growth of $(\text{NH}_4)_2\text{SiF}_6$ crystals when Si wafer is exposed to the vapor of $\text{HNO}_3:\text{HF}$ chemical mixture [1]. It is likely that this exposure induces oxidation on the wafer surface following the reaction $4\text{Si} + 6\text{HF} + 2\text{HNO}_3 \rightarrow (\text{NH}_4)_2\text{SiF}_6 + 3\text{SiO}_2$. But it is also required for the growth of $(\text{NH}_4)_2\text{SiF}_6$, hence the name seed layer is due. Figure 1 shows the cross-sectional image of such a growth process and the energy dispersive x-ray (EDX or EDS) measurements to determine the concentration distribution of elements. Ammonium silicon hexafluoride crystal layer is about $100\ \mu\text{m}$ thick as a result of several hours of growth, the seed layer has almost fixed thickness of about sub-micron. Also shown is the distribution of elements throughout the cross section from the surface to the wafer. The green curve is typical density distribution of Si atoms, picking at the interface around the seed layer. This peak is followed by a dip within the wafer and then reaches a constant value deep inside wafer, which could be due to silicon consumption during the $(\text{NH}_4)_2\text{SiF}_6$ formation. The insert indicates the fluorine concentration, which is relatively high in the $(\text{NH}_4)_2\text{SiF}_6$ as expected (yellow color). The metals such as Ta and Al are due to surface metallization but their concentration is almost negligible. From the weighted ratio, the x was determined to be 1.74 in silicon sub-oxide layer, SiO_x .

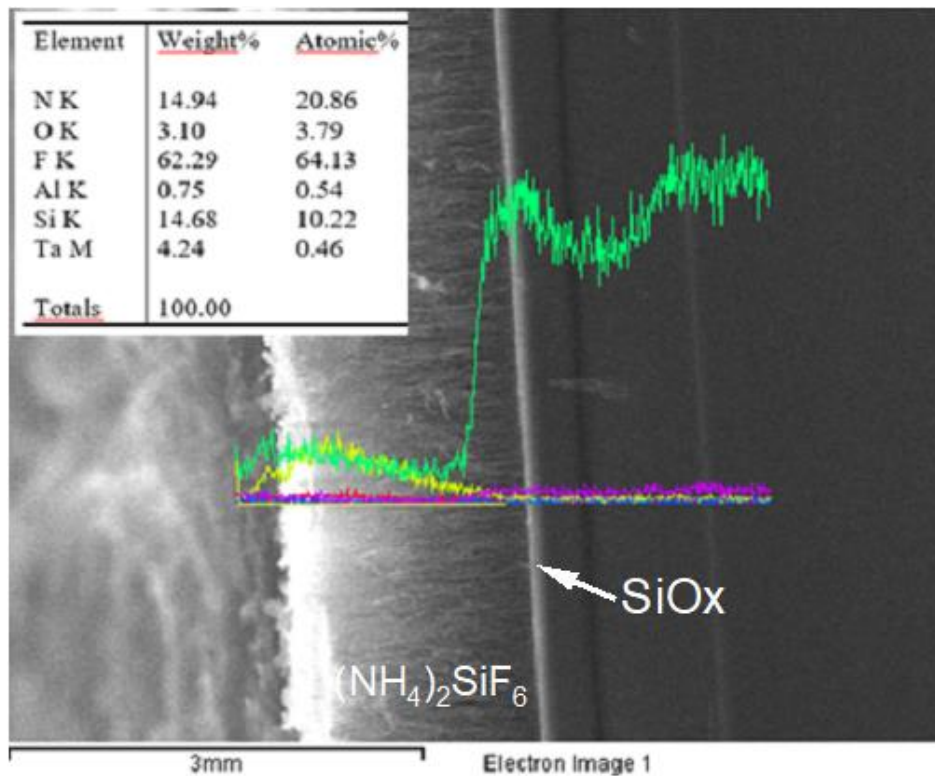


Figure 1 EDX spectrum taken from the cross-section of the sample indicating the distribution of elements. Colored line indicates Silicon (green line) and Fluorine (yellow line). Elements and atomic concentrations are shown in the insert.

2.2 Scanning probe analysis

Results of the Atomic Force Microscopy, AFM, measurements are shown in Fig. 2. The seed layer with the scan area of $1 \times 1\ \mu\text{m}^2$, prepared with 10% HF and 42% HNO_3 for 4 hours indicate a porous-like surface structure. In Fig 2(b), the height histogram indicating a roughness of $\text{RMS} = 33.9\ \text{\AA}$ and the bearing curve indicates a relatively smooth surface with occurrence of peaks and valleys.

The bearing curve gives the areal material ratio under the profile at any given depth as compared to a perfectly flat profile. The parameters marked on the curve indicate the core roughness R_c (50 nm), reduced peak height R_p (40 nm) and the reduced valley depth R_v (40 nm), respectively.

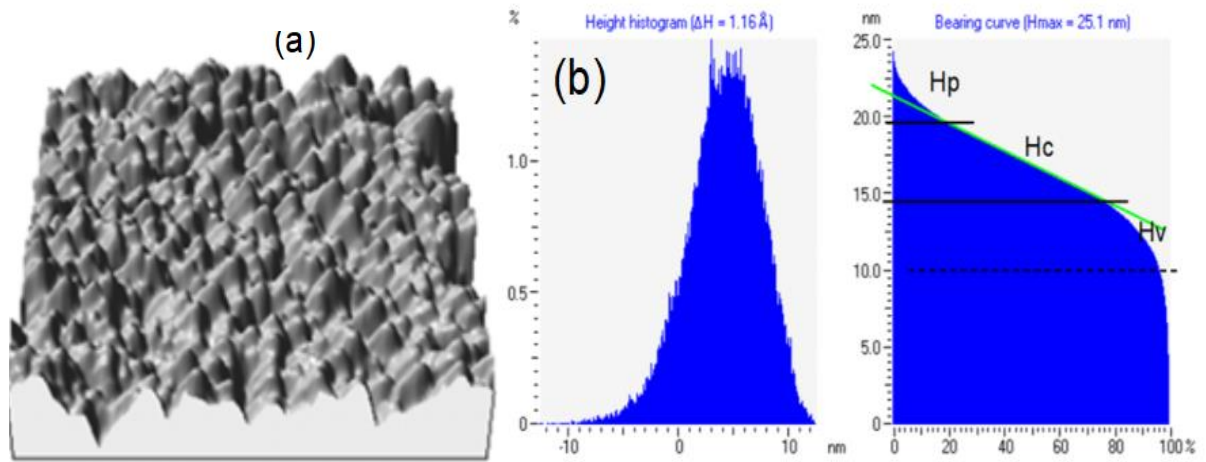


Figure 2(a) 3D AFM topography image of the seed layer with the scan size of $1 \times 1 \mu\text{m}^2$, prepared with 10% HF and 42% HNO_3 for 4 hours; b) The height histogram indicating a roughness of $\text{RMS} = 33.9 \text{ \AA}$ and the bearing curve.

3. RESULTS AND DISCUSSION

3.1 Fourier Transformed Infrared spectroscopy: Si-O-Si stretching modes

The localized vibrational modes related to Si-O-Si stretching frequencies are represented in Figure 3. For oxides grown on plane wafer, the frequency of these modes appear at around 1100 cm^{-1} as a doublet at 1081 cm^{-1} and 1185 cm^{-1} (solid red line). The spectrum is compared to that of DI water rinsed sample having the lower frequency mode shifted by 5 cm^{-1} and the higher frequency is smoothed (solid black line).

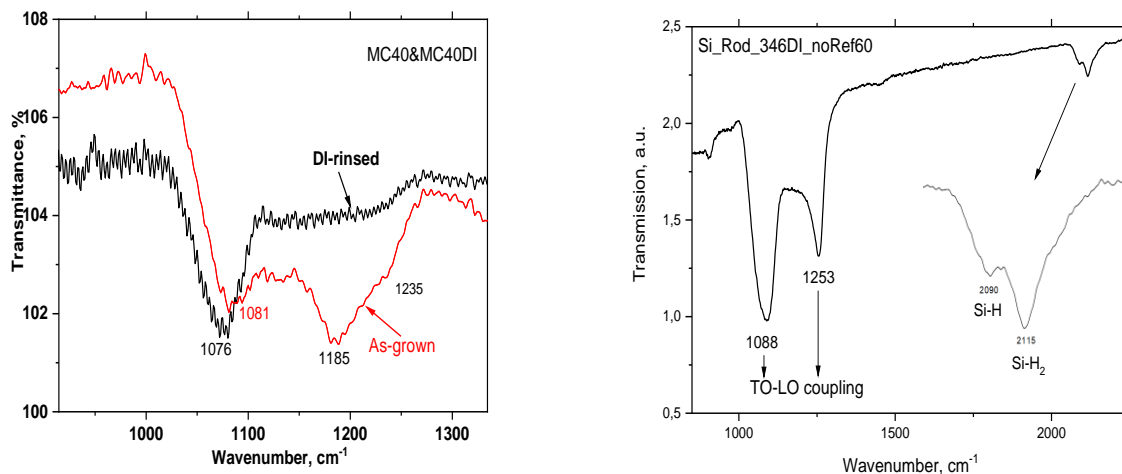


Figure 3 Infrared vibrational modes of Si-O-Si bonding. (a) Si-O-Si stretching vibrations of an as grown oxide compared with the same sample after DI water rinsing, (b) Oxide vibrations measured on Si wafer consisting of Si rods of 400 nm in diameter. The insert indicates the presence of Si-H and Si-H₂ modes.

In Fig. 3(b), we observe the splitting of Si-O-Si vibrational bands due to transverse-optic (TO) and longitudinal-optic (LO) modes coupling [1, 2]. The forming rods on Si surface increases the surface area, which in turn enhances the splitting of LO-TO coupling modes. The vibration that we observe at 1076 cm⁻¹ belongs to optically active oxygen asymmetric stretch TO mode (in-phase motion of adjacent oxygen atoms). The coupling can be experimentally measured by in oblique incidence p-polarized transmission spectrum as peaks at around 1076 – 1253 cm⁻¹ on Si wafers [2].

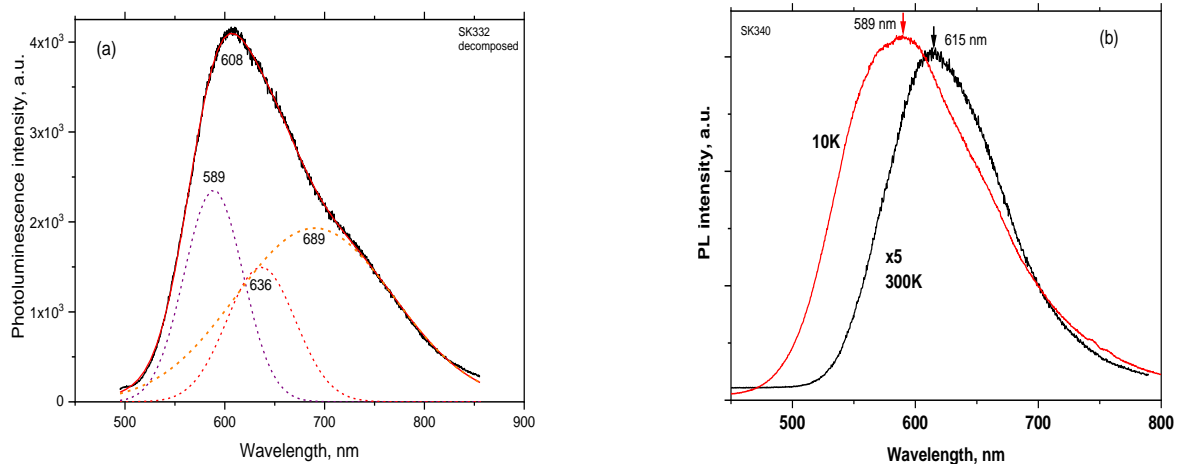
Another important feature of the spectrum is the incorporation of Hydrogen atoms into SiO_x matrix as evidenced from the FTIR spectrum in Fig. 3(b), at around 2000 – 2200 cm⁻¹. These vibrations are attributable to Si-H_n (n=1, 2, 3) modes [3]. Note that this incorporation occurs only under certain preparation conditions.

3.2 Photoluminescence

3.2.1 Continuous wave (CW) photoluminescence (PL)

CW PL measurements have been performed at room temperature and at low temperature 10K using an Ar ion laser of 514 nm. The results are shown in Fig. 4 for temperature and surface condition dependent behavior. Using the equation of the Gauss model, photoluminescence emission curve can be fitted by the following equation, resulting in peaks at around 690 nm, 630 nm and 590 nm. Broad band peaked at around 608 nm can be de-convoluted into three emission bands peaked at 689 nm, 636 nm and 589 nm. A number of studies have carried out on Si nanocrystals and the origin of the emission peaks from about the Si band-gap (1.1 eV) to higher energies have been attributed to quantum confinement effects [4]. These PL emissions from the various size nanocrystals were named as S-band emission and our peaks at 1.8 eV (689 nm), 1.95 eV (636 nm) and 2.1 eV (589 nm) would correspond to nanocrystals with average diameter of 2.6 nm, 2.3 nm and 1.8 nm, respectively.

The shape and the location of the PL emission bands vary depending on the preparation conditions. For example, the band at 615 nm at 300 K in Fig. 4(b) shifts to higher energies, 2.1 eV at the low temperature, 10 K. Also, a broadening of %40 in low temperature PL was observed with respect to 300K spectrum. This broadening can be attributed to the activation of additional nanocrystals as the temperature is lowered. Another interesting feature is the initial steps of the oxide formation as shown in Fig. 4(c), where the PL peaks at 740 nm for 1 minute exposure time and shifts to higher energy, that is 735 nm for 80 seconds of exposure. A second band appears also as a shoulder at 770 nm at short exposure time. The results indicate that the PL emission bands moves to higher energies with the processing time. Fig.4(d) summarizes the incidences of observed main PL peak positions for a number of samples.



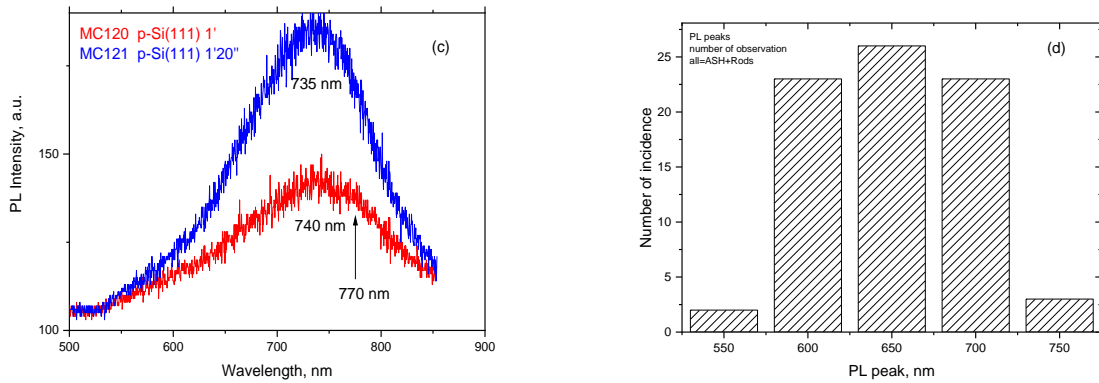


Figure 4 CW photoluminescence of SiOx seed layer measured under different surface conditions. (a) The plane surface, (b) temperature effect, (c) initial oxide growth, (d) incidence of PL peaks on a number of SiOx seed sample.

3.2.2 Time-resolved photoluminescence

The temporal and spectral dependence of the SiOx seed layer are shown in Fig. 5 (a) and (b). The PL emission was obtained at 300 K between 470 nm and 600 nm using 400 nm (3.1 eV) excitation line of a Ti-Sapphire laser with a power levels up to 8 mW. The intensity distribution was deduced by steak camera image.

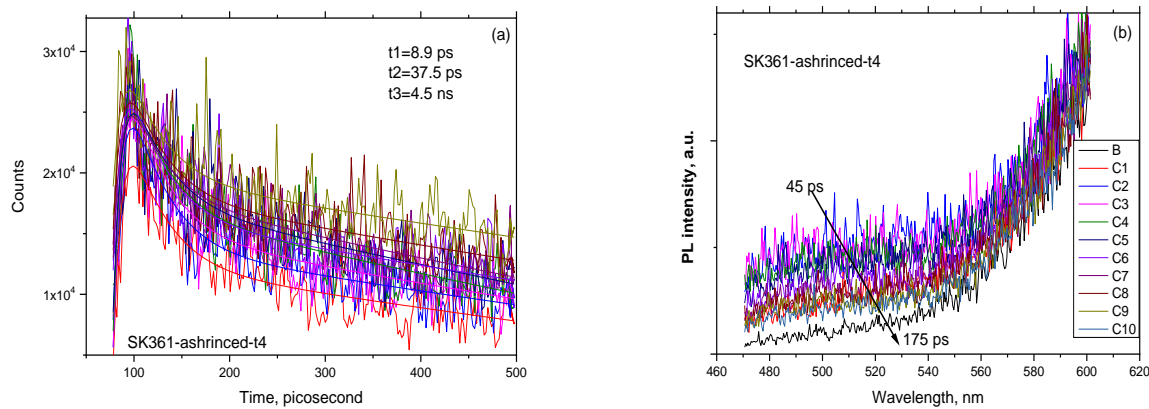


Figure 5 Temporal and spectral characteristics of the time-resolved photoluminescence measurements

The temporal curves have been fit using a simulation program resulting in three components lifetimes as typical dynamical behavior as shown in Fig. 5(a). The following expression was found to be well describing the luminescence decay time

$$I = \sum_i A_i \exp(t / \tau_i) \quad \text{where } i = 1, 2, 3 \text{ and } A_i \text{ is a constant and } \tau \text{ is the lifetime of carriers.}$$

The results of this analysis reveal three different lifetimes or decay components: 8.9 ps, 37.5 ps and 4500 ps, which can be attributed to ultrafast recombination of carriers at nanostructured Si, at silicon-oxide interface and oxide color centers, respectively. However, we don't exclude the attribution of these emissions originating from nanostructured silicon of different sizes leading to the quantum confinement of carriers. By analogy to previous studies, the short lived states related emission is due smaller size crystals and the long lived states could be attributed to larger crystals [4].

The time dependence of the spectral distribution of the emission is shown on Fig. 5(b) from 45 ps to 1975 ps time frame. The emission intensity decreases with time at shorter wavelengths, indicating the charge transfer to long lived states, that is red emission region.

3.3 Spectroscopic ellipsometry (SE)

The second order derivative of spectroscopic ellipsometry measurement for a SiOx seed layer is shown in Fig. 5, where interband critical electronic energy points, E1 (3.4 eV) and E2 (4.3 eV) are indicated. These critical energy points are typical of crystalline silicon, hence originating from the wafer [5]. The features at higher energies, that is 4.6 eV and 4.8 eV are rather attributable to some structural disorder and irregularities, if not quantum confinement effect at smaller size silicon nanostructures.

The SE of the initial stages of the SiOx formation is represented by Fig. 5(b). There are very sharp peaks at relatively lower energies, 1.35 eV and 1.65 eV, which would correspond to nanocrystal sizes of 5.4 nm and 2.5 nm, respectively, if we considered a quantum confinement effect [4].

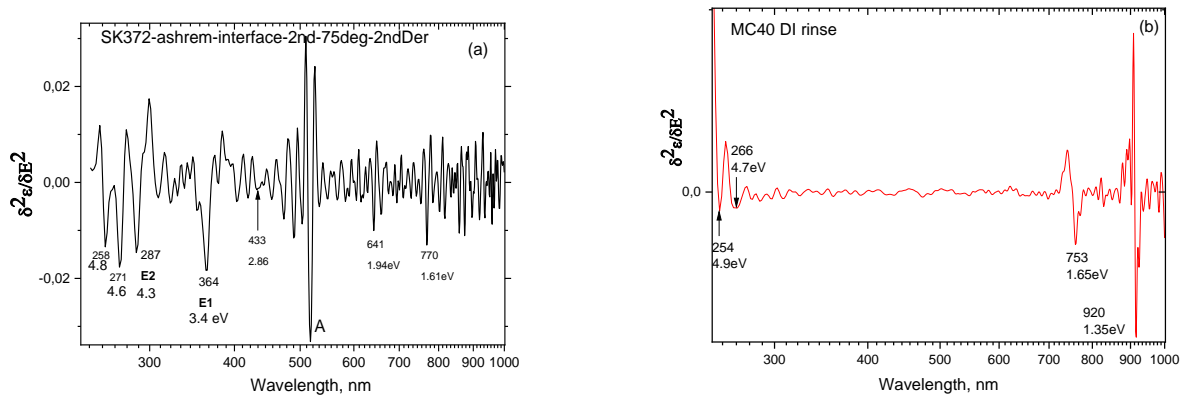


Figure 6 The second derivative of the spectroscopic ellipsometry measurement taken on SiOx. The peak A is an experimental artefact.

3.4 Resistive switching properties

Resistive switching characteristics of the SiOx seed layer are shown in Fig.7 on consecutive voltage sweeps. I-V measurements were performed using Keithley 4200 Semiconductor Parameter Analyzer system and a probe station at room temperature. The measurements were done on devices with 50 nm Pt top electrode. Silicon wafer was used as bottom electrode.

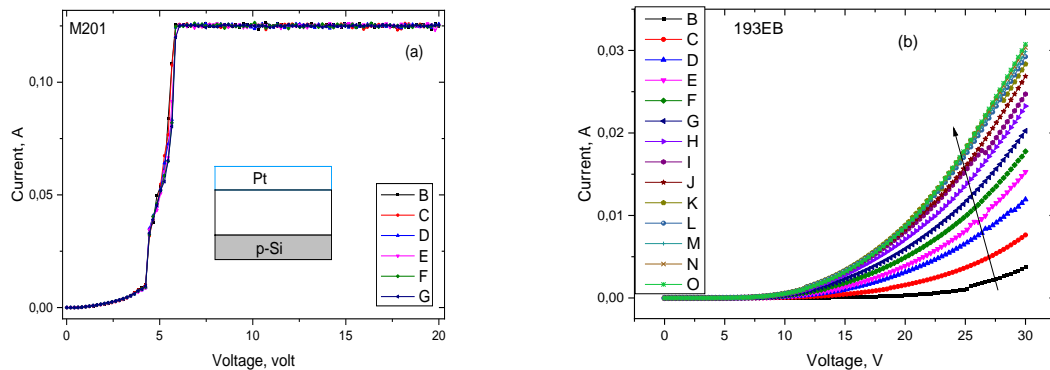


Figure 7 Resistive switching properties: analog switching characteristics on consecutive voltage sweeps. (a) The electroforming in a Pt/SiOx/p-Si device. (b) Under positive sweep indicating the increase of the conductance in SET process.

As shown in Fig. 7(a), the forming starts at around 4 V with a double forming steps for this particular sample. Upon consecutive sweeps, the same characteristic was reproduced. The saturation of the current at higher voltages is due to the compliance current set at 150 mA. Resistive switching or forming in silicon suboxide was found to be an intrinsic property of the suboxide. It has been proposed that the switching mechanism is driven by competing field-driven formation, and current-driven switch-off the conductive filament [6, 7]. The switchable conductive pathway was demonstrated to be due to trap assisted tunneling through silicon nanocrystals embedded within the seed layer.

Fig. 7 (b) is the current-voltage characteristics indicating the increase in conductance after successive SET process. This behavior can be attributed to the fact that the forming process is not completed.

CONCLUSION

A comprehensive description of the physical and electrical properties of the silicon suboxide layer formed during the ammonium silicon hexafluoride crystals was provided in this work. The porous-like surface structure as determined by scanning probe analysis provided 3D image of the nanostructured morphology with an RMS value of few nanometers. The presence of TO-LO coupling of asymmetric stretching modes of Si-O-Si bonding and the activation of this coupling was clearly demonstrated. The sample preparation conditions can be arranged to incorporate hydrogen atoms into the suboxide matrix as evidenced by localized Si-H vibrational modes.

The suboxide layer exhibits an efficient photoluminescence emission in the region from blue to 900 nm with an average peak PL energy at around 650 nm but with a shift down to 500nm and up to 800 nm. The low temperature PL indicates an enhancement in the emission intensity, which accompanied by a blue shift. The emission bands can be associated with the quantum sized silicon crystals. The critical energy points as deduced from spectroscopic ellipsometry are compatible with the PL and quantum confinement effects.

The lifetime measurements are indicative of ultrafast components in the low range of picosecond regime, which could be associated with the radiative recombination in the smallest size nanostructures, in which electron and hole wave functions are most overlapped. Also, a charge transfer to long lived states enhances red emission with a longer decay time.

Concerning resistive switching properties, the presence of forming is well observed, suggesting the possibility of application as resistive non-volatile memories, ReRAM. We think that the suboxide switching would perform best when the device is fabricated on a SOI wafer.

Acknowledgement

This work did not receive any specific grant from funding agencies. It was supported by European Commission LASERLAB-EUROPE program (LLC001765) and MC2ACCESS for facility use and Ö. Arthursson for AFM probing of surfaces. We thank Prof. W. Sunström for the access to Lund Laser Center and Dr.A.E. Hannas for the assistance in femtosecond laser measurements. BMBF and TUBITAK are acknowledged for the bilateral program and Dr. P. Werner and Dr. V. Talalaev for fruitful discussions and low temperature photoluminescence measurements.

REFERENCES

- [1] Kalem, S., "Synthesis of ammonium silicon fluoride cryptocrystals on Silicon, Applied Surface Science 236, 336(2004) <http://arxiv.org/abs/cond-mat/0410606>
- [2] Kirk, C.T., "Quantitative analysis of the effect of disorder-induced mode coupling on infrared absorption in silica", Phys. Rev. B38, 1255 (1988).
- [3] Kalem, S. et al., "Infrared spectroscopy of hydrogenated and chlorinated amorphous silicon, Phil. Mag. 53, 509(1986). <https://arxiv.org/ftp/arxiv/papers/2110/2110.03770.pdf>.

- [4] Canham, L., "Origins and applications of efficient visible photoluminescence from silicon based nanostructures", Royal Society of Chemistry, Faraday Discuss., 222, 10 (2020).
- [5] Petrik, P. et al., "Nanocrystal characterization by ellipsometry in porous silicon using model dielectric function", J. Applied Physics 105, 2(2009).
- [6] Mehonic, A. et al "Resistive switching in silicon suboxide films" J. Applied Physics 111, 074507 (2012).
- [7] Buckwell, M et al., "Neuromorphic Dynamics at the Nanoscale in Silicon Suboxide RRAM", Frontiers in nanotechnology 3, 699037 (2021).